Animals identify and discriminate odors using olfactory receptors (Ors) expressed in olfactory receptor neurons (ORNs) [1, 2]. In both insects and vertebrates, distinct ORNs, which typically express a single Or, respond broadly to many distinct volatile odorants [3–8]. Likewise, any given odorant may incite strong responses in a number of ORNs. ORN tuning curves are therefore broad and overlapping, implying that odors are encoded combinatorially – by the particular combination of responses they elicit in the ORN repertoire, patterns which are eventually decoded downstream into behavioral response [9].

Odor signals in nature are uniquely complex in composition, space, and time, and like other sensory modalities, olfactory systems must tune their response to the character of input stimuli [10–14]. Various features of natural odor signals are power-law distributed, producing whiffs of widely varying duration and intensity [12]. Sensitivity to low concentrations could thus lead to saturation at high intensities, confounding combinatorial representations of odor identity. Further, ethologically-relevant odors are often mixed together with nuisance odors; due to the non-specificity of ORN response, distinct odors could simultaneously activate overlapping ORN subsets, preventing accurate disambiguation [15].

What invariances and adaptive mechanisms might help preserve combinatorial odor representations in natural environments? In *Drosophila* larvae, dose responses of 324 OR-odorant combinations obey a single activation function shape, with similar Hill coefficients but different activation thresholds, which are distributed as a power law [16]. *Drosophila* ORNs also exhibit a large degree of similarity in their temporal integration of fluctuating stimuli. While for some Or-odor combinations, ORN response can exhibit large differences, such as super-sustained responses [17], deconvolution of stimulus dynamics from neuron responses produces stereotyped filters that differ little among ORNs [18].
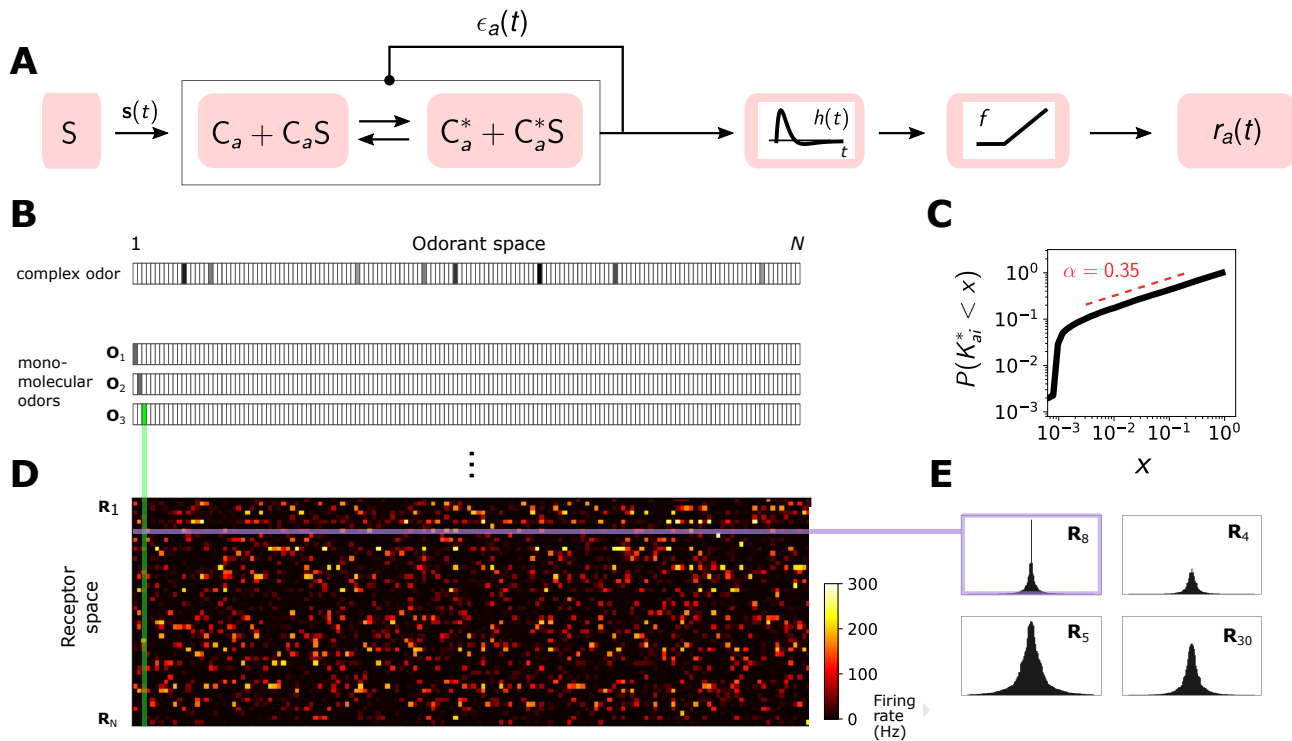
Beyond these invariances are adaptive mechanisms which can preserve odor representations amid environmental changes. In *Drosophila*, antennal lobe glomeruli receiving connections from ORNs send mutually inhibitory connections, effectively normalizing incoming ORN signals before they are projected to the lateral horn and mushroom body [19, 20]. In the mushroom body, inhibition from giant interneuron upon Kenyon cells further acts to suppress patterns of activity elicited by these odors [21]. Further, upstream of these connectivity-mediated mechanisms, individual ORNs themselves adapt in time an apparently universal way: ORN gain varies inversely with mean odor concentration according to Weber's Law of psychophysics [22], while maintaining response time independent of odor intensity [14, 23, 24]. Weber's Law has been observed in several OR-odorant combinations, and is traced to feedback mechanisms operating at the level of odor transduction, upstream of ORN firing machinery [14]. This points to a mechanistic origin involving modification of phosphorlyation sites on the universal *Drosophila* co-receptor Orco. Other phosphorylation sites on Orco have been implicated in desensitization to odors over longer timescales as well [25, 26].

While in a single channel system such as *E. coli*, adaptive feedback via Weber's Law is known to robustly maintain sensitivity in response to mean concentration changes, the implications for a multiple-channel system – which combines information from several sensors with overlapping receptive fields – is less straightforward. Here we combine a biophysical model of universal ORN adaptive response and neural firing with various sparse signal decoding frameworks to explore whether and how ORN adaptation maintains accurate combinatorial coding of odor signals that span varying degrees of intensity, molecular complexity, and temporal structure. We find that front-end gain modulation helps preserve coding capacity within the non-specifically sensing ORN repertoire, and maintains abstract representations of odor identity across different intensities. As such, this adaptive mechanism promotes the accurate discrimination of weak odor signals from strong backgrounds of varying molecular complexity, both in static odor environments and in fluctuating ones. We also investigate the predictions of our model for the *primacy coding* hypothesis – that odors are encoded entirely by the subset of a few earliest responding ORNs [27, 28]. Our results agree with primacy coding when odor signals are sufficiently simple, though signals composed of more molecular constituents require the recruitment of the full ORN repertoire. Finally, we show that front-end adaptation acts in concert with divisive normalization in the antennal lobe to maintain the invariance of activity patterns in the mushroom body. Together, our results suggest that despite the broad overlap of ORN tuning curves, a universal mechanism of front-end adaptation may play a vital role in preserving representations of odor identity in naturalistic odor landscapes.

1. Results

A. Model of ORN sensing repertoire. Odor identification consists of encoding in the sensing periphery followed by decoding in higher-level processing centers of the olfactory circuit. We first examine how front-end adaptation can maintain odor encoding capacity, by drawing upon a model of odor-to-ORN firing recently shown to reproduce experimental findings: Weber-Fechner scaling, signal transduction kinetics, and firing rate dynamics of individual *Drosophila* ORNs to fluctuating stimuli [14]. Here we generalize this model to a repertoire of $M = 50$ ORN types. ORNs house olfactory receptor complexes C_a, $a = 1, ..., M$, each consisting of an ORN-specific OR and the universally-expressed olfactory co-receptor Orco, which mediates odor transduction through dendritic localization of and heteromerization with ORs (Fig. 1a). These odorant-response functional units interact with odor mixtures, each of which is composed of some combination of N odorant molecules with time-dependent concentrations $s_i(t)$, $i = 1, ..., N$ (Fig. 1b). We choose $N = 150$, as this number is sufficiently larger than the size of the sensing repertoire M. Functionally, C_a forms a non-selective cation channel whose current is mediated by the strength and nature of bound ligands. We thus model a given complex as stochastically switching between active (channels open) and inactive states, while also being bound or unbound with odorant i. The active conformation binds odorant i with higher affinity than the inactive conformation, resulting in distinct dissociation constants, K_{ia}^* and K_{ia}, respectively. In steady state, the active fraction A_a of Or/Orco complexes in

Lead author last name *et al.*

PNAS | **September 19, 2018** | vol. XXX | no. XX | **1**

125
126
127
...
187
188
189

Fig. 1. **A** Odor binding model. Or/Orco complexes C_a bind odorant molecules s_i comprising stimuli S. These complexes can stochastically switch between inactive and active states, where the steady-state active fraction is determined by the complex free energy $\epsilon_a(t)$. The activity feeds back on to the free energies with timescale τ_a to pull the activity to a baseline level A_{a0}. ORN firing rates $r_a(t)$ are generated by passing $A_a(t)$ through a linear temporal filter $h(t)$ and a nonlinear thresholding function f. **B** Odor mixtures are represented by real-valued N-dimensional vectors $\mathbf{s}$, whose components s_i are the concentrations of the individual molecular constituents of $\mathbf{s}$. **C** Following (), active binding constants are distributed as a power-law with coefficient $\alpha = 0.35$ **D** The maximal firing response of 50 ORNs to the 150-possible monomolecular odors $\mathbf{s} = s_i$, for the power-law K_{ai}^* distribution in C. **E** Representative ORN tuning curves, generated by ordering the responses within a single row of the response matrix in D. A diversity of response, mimicking that of (6), arises from both the distribution of odorant binding constants K_{ai}^* and the distribution of receptor free energies ϵ_a.

ORN a can be solved for as (see Methods):

$$A_a(t) = \left(1 + e^{\epsilon_a(t)}\right)^{-1}$$
$$\epsilon_a(t) = \epsilon_{a,\text{act}}(t) + \epsilon_{a,\text{ligand}}(t)$$
$$\epsilon_{a,\text{ligand}}(t) = \frac{1 + \sum_i^N s_i(t)/K_{ai}}{1 + \sum_i^N s_i(t)/K_{ai}^*}, \qquad [1]$$

where $\epsilon_{a,\text{act}}(t)$ is the free energy cost of C_a activation. NAT LOG

Inward currents elicited by activation of the Or/Orco receptor complexes then incite firing activity in ORNs. Following (14), we model the Or/Orco-to-ORN transformation with a temporal filter followed by rectifying nonlinearity f (see Methods):

$$r_a(t) = f\left(\int h(\tau - t)A_a(t)d\tau\right). \qquad [2]$$

At the single ORN level, this nonlinear-linear-nonlinear framework (Or/Orco activation → temporal filter → nonlinear rectifier) reproduces Weber Law gain adaptation and signal transduction kinetics, notably the temporal slowdown of the local field potential upon adaptation, along with a complementary speed-up in the firing machinery.

Here $\epsilon_a(t)$ represents the free energy change due to modifications of the Or/Orco complexes by adaptation. Opening of the channels causes an inward current that eventually results in a negative feedback onto $A(t)$. This is modeled minimally by:

$$\frac{d\epsilon_a(t)}{dt} = \frac{A_{a0} - A_a(t)}{\tau_a} \qquad [3]$$

within the finite range $\epsilon_{L,a} < \epsilon_a(t) < \epsilon_{H,a}$. It has been shown that when properly deconvolved from the stimulus dynamics, the shape of temporal kernels in adult *Drosophila* ORNs is largely odor-independent, though may differ by brief ($\sim$10 ms) odor-dependent delays (18). Accordingly, we model $h(t)$ by an ORN- and odor-independent double-exponential function, with parameters matched to experiment (18). We assume that the lower cutoffs $\epsilon_{L,a}$ are receptor-dependent and choose them from a normal distribution. This variability ensures that ORNs are activated above quiescence (around 5 Hz) at distinct stimulus levels (14).

Diversity among maximal odor-ORN response arises from the distribution of chemical affinities, encapsulated in K_{ai}^*. We choose these from a power law distribution ($\alpha = 0.35$), as was recently found across ORN-odor pairs in *Drosophila* larvae (Fig. 1c). To mimic the presence of private odors relevant to innate responses, we manually add a high responder ($K_{ai}^* \sim$ small) to a handful of ORNs; the addition of these private odors did not affect the general findings. Together, the power-law distributed K_{ai}^*, receptor-dependent $\epsilon_{L,a}$, and invariance in temporal filters, when incorporated into the steady-state model responses Eq. 1, produce tuning curves mimicking the maximal

Lead author last name *et al.*

PNAS | **September 19, 2018** | vol. XXX | no. XX | **3**
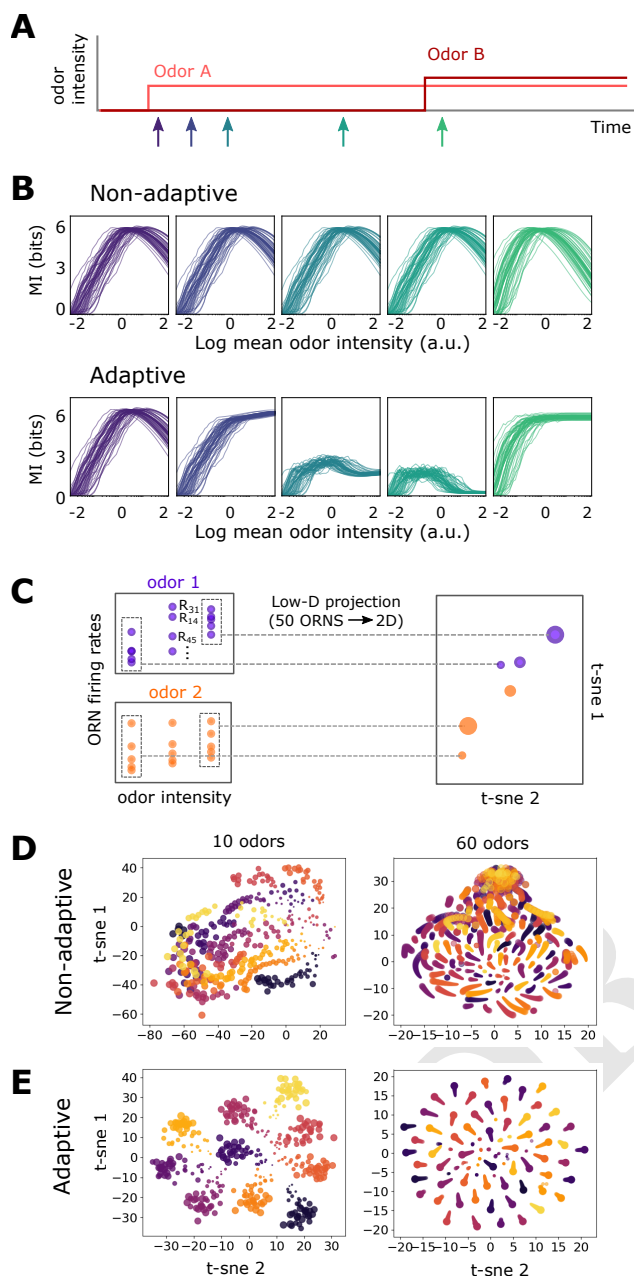
Fig. 2. Front-end adaptation maintains information capacity and representations of odor identity across changes in intensity. **A** Evolution of mutual information (MI) between odor signals and ORN response, as a function of relative odor concentration. Odor A arrives at t_1 and Odor B (of similar intensity) arrives at t_2, where $t_2 - t_1 \gg \tau_A$. MI is plotted for both an unadaptive and adaptive system at times of order of τ_A following t_1 (purple; purple-blue), right before t_2 (blue-green), and shortly after t_2 (green). **B** To investigate abstract representations of odor identity in the ORN response, ORN responses are projected from 50 dimensions to 2 dimensions, using nonlinear dimensionality reduction. In the 2D space, distinct odors are plotted as points of distinct colors, and point size represents odor intensity. **C** In the adaptive system, responses cluster by identity more apparently for an adaptive system (bottom row), than a non-adaptive system (top row), shown here for 10 and 60 sparse odor identities for several concentrations each.

Drosophila ORN responses to many individual odorants (6) (Fig. 1d-1e).

B. Concentration-invariant preservation of coding capacity and abstract representations of odor identity.

To investigate the dependence of encoding capacity on odor concentration, we calculate the mutual information (MI) between odor signals $\mathbf{s}$ and responses $\mathbf{A}$ in two sensing systems, one with ORN adaptive feedback (via Eq. 3) and one without. We consider a simple situation, in which a step of odor A, $\mathbf{s}_A$, turns on at time t_1, persists for some time, and then odor B, $\mathbf{s}_B$ (a distinct identity) turns on at some later time t_2. For simplicity, we assume that both odors have similar intensities $s_0 = \langle s_i \rangle$ and calculate the MI between the ORN responses $\mathbf{r}_a$ and signals $\mathbf{s}_A + \mathbf{s}_B$ at various times after t_1, as a function of s_0. In the non-adaptive case, MI peaks around the region of maximum sensitivity ($\sim 10^2$ a.u.) after t_1 (Fig. 2a). ORNs are firing at an elevated rate, however, more susceptible to saturation with further odor onsets. Thus, following t_2, the maximum shifts leftward as odors of high intensities have saturated the system and cannot pass any more information.

The adaptive system mimics the non-adaptive system at t_1, before adaptation has kicked in (Fig. 2a). As the activity feeds back onto ϵ_a, the response to higher concentrations passes through the regime of high sensitivity, and the MI peak shifts rightward. Over time, the responses for all signals have reached the baseline firing rate, and the mutual information is mostly eliminated since the firing rate is independent of odor identity. However, having now adjusted its regime of maximum sensitivity to the presence of odor A, the system can respond appropriately to odor B: the MI at t_2 is nearly 6 bits across 3 decades of concentration, in contrast to the non-adaptive case. These results suggest that in this multi-channel compressive system, a simple mechanism of universal integral feedback can help maintain sensitivity in changing environments.

We expect that this preservation of information capacity might therefore help maintain abstract representations of odor identity. To examine such representations, we project the ORN response repertoire to a lower dimensional space using t-distributed stochastic neighbor embedding (t-SNE), a nonlinear, local dimensionality reduction technique (29). Here, each data point is a 50-dimensional vector representing the ORN firing responses to a given odor of a given intensity. Each of these data points is then reduced by t-SNE to two dimensions (Fig. 2b). Testing this both for a smaller odor repertoire (10 odor identities) and a larger one (60 identities), we find that odors separate by identity in the adaptive system, while in the unadaptive system, representations mix among their identity and concentration (Fig. 2b). Together, these results suggest that at the level of ORN response, front-end adaptation helps maintain representations of odor identity across changes in odor intensity.

C. Front-end adaptation promotes odor discrimination accuracy in static and fluctuating environments.

Next, we ask how the universal adaptive feedback might contribute to accurate signal reconstruction from ORN responses. One potentially complicating factor is the disparity between sensor dimension and stimulus dimension: while *Drosophila* only express ~ 60 olfactory receptor genes (30), the space of aromatic odorants is far greater (31). However, many naturally-occurring odors are comprised of only a small subset of these volatile compounds – they are sparse in the space of odorants (31). This is suggestive as mathematical results in compressed sensing

guarantee the reconstruction of these sparse signals, assuming a sufficiently random response (32–34). While at this stage of the analysis we use a compressed decoding framework, there is no evidence that this algorithm is being implemented in the *Drosophila* olfactory circuit (35), and we later verify our conclusions with other classification techniques.

To incorporate the linear framework of compressed sensing into our nonlinear encoding model, we treat the odor encoding process exactly, while approximating the decoding to first order. We denote an odor signal as accurately decoded if both (i) the sparse components are all estimated within some tolerance of their true values, and (ii) the estimates of components not in the odor mixture ("zero" components) are sufficiently low (see Methods).

To gauge the impact of universal front-end feedback on odor discrimination, we apply this scheme to a static odor mixture containing two sparse odors, which we call the "foreground" and "background". We ask how well the foreground can be decoded in the presence of backgrounds of given intensity and molecular complexity. In the unadaptive system, accuracy in the regime of maximum sensitivity is maintained if the background concentration is low enough, but is compromised as intensity increases (Fig. 3c). For higher background concentrations, molecular complexity also has a more damaging effect on decoding accuracy. Finally, for sufficiently strong and complex backgrounds, the foreground is virtually undetectable (top right plot in Fig. 3c). The adaptive system is substantially more robust (Fig. 3d), although the minimum detectable concentration does increase with background intensity.

Realistic odor environments are highly variable, with odor concentrations and whiff durations that can span several orders in a short time (12). We next wondered whether a single OR/Orco adaptation timescale ($\tau_A \sim 250$ ms (14)) could promote whiff detection in such environments. We apply our coding framework to a recorded time trace from a photo-ionization detector placed downwind of an odor source (Fig. **??**). This trace serves as the odor intensity, to which we randomly assign a sparse identity from the N-dimensional odorant space. To investigate discrimination accuracy, we add to this a static background odor signal, and then calculate the percentage of decoded whiffs. Finally, we mimic a finite length of short-term memory, such that only changes in detected odor signal are remembered, and only for τ_F seconds in the past.

Without ORN adaptation, sufficiently strong backgrounds eliminate whiff-detection ability, irrespective of the complexity of either the foreground or background odor (Fig. **??**, green lines). In the adaptive system, this is substantially mitigated, (red lines in Fig. **??**) although accuracy does decrease in general with increasing background complexity. Further, accurate whiff detection requires τ_F only on the order of τ_A (darker red lines), indicating that a universal timescale of ORN adaptation promotes detection of naturalistic odor signals amidst confounding backgrounds.

D. Relationship to primacy coding hypothesis. An intriguing emergent hypothesis, "primacy coding," posits that odor identity is encoded entirely by the set (but not order) of the p earliest responding glomeruli, called "primacy sets" of order p (Fig. 4a). Primacy sets would in principle comprise a concentration-invariant representation of odor identity. In our framework, odors are decoded via information passed simultaneously from all 50 ORNs. However, some of this information
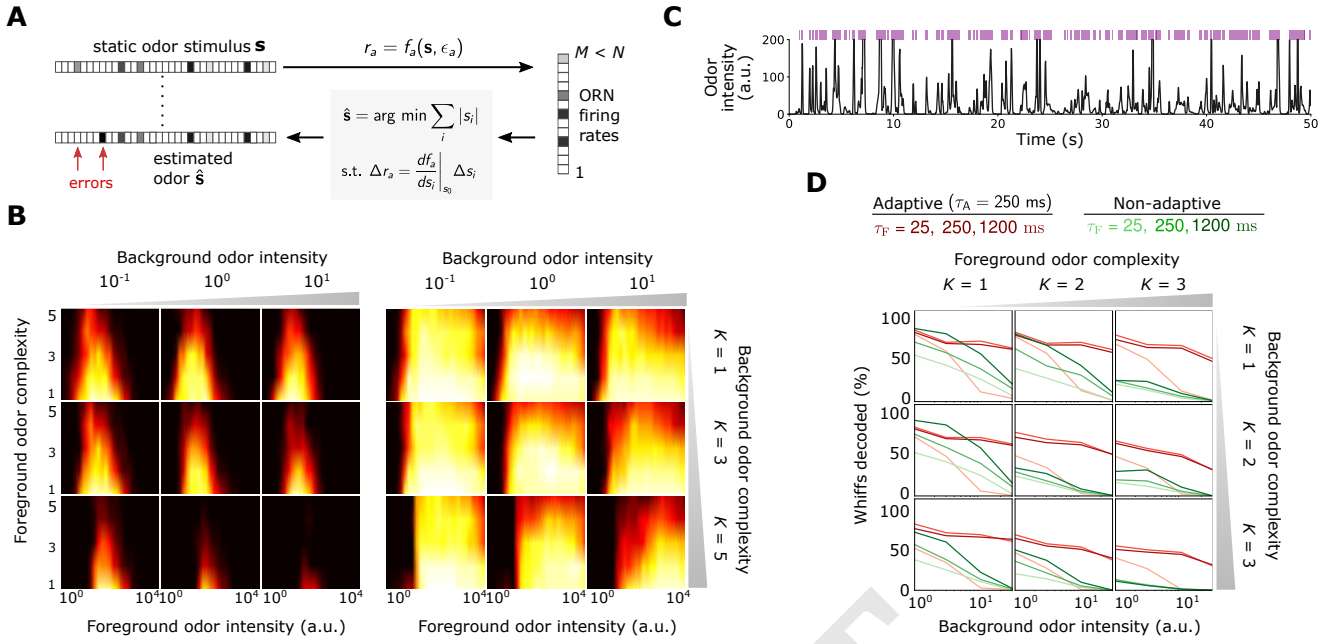
may be redundant, whereby a set of earliest active ORNs are sufficient for odor recognition; if so, our theory would generate predictions in agreement with primacy coding. To test this, we consider a steep sigmoidal stimulus with half-max slope of $1/50$ ms^{-1}, as in Fig. 4a. We calculate the decoding accuracy as a function of time, and plot in Fig. 4b the accuracy as a function of number of active ORNs, which increases monotonically as the signal rises (Fig. 4a). To illustrate how the recruitment of ORNs incrementally improves odor signal recognition, we allow for partial accuracy by calculating the percentage of correctly decoded individual odor components.

For sufficiently simple odors, our results are indeed in accordance with primacy coding: the set of earliest responding neurons fully account for the odor identity ($K = 1, 3, 5$ plots in Fig. 4b). Though all ORNs eventually activate as the stimulus increases, the latter responders confer no further information in odor recognition. As expected, the active ORN subset comprising the primacy set is distinct for each odor, Show that recruited ORNs are all distinct. We do find, however, that for more complex odor mixtures, the full ORN repertoire must be active for accurate decoding ($K = 7, 9$ plots in Fig. 4b), a result that holds across odor odor concentrations (Fig. 4c). In this regime, there can be no primacy code, since a primacy set consisting of the full ORN repertoire would encode only a single odor. Conversely, our framework can decode the odor for a maximal primacy set since it utilizes not just the identity of the active ORNs, but also their individual firing responses. Primacy coding also predicts that for stronger stimuli, behavioral responses shift earlier in time, since the primacy set is activated quicker. We calculate this time shift and find that it rises monotonically with odor intensity over a decade of concentrations.

Primacy sets are inherently concentration-invariant. But to what extent are they conserved among varying environmental conditions, such as persistent background odors? ORNs that have adapted their gain in response to a background odor could in principle be pushed out of the primacy sets of a novel odor due to reduced sensitivity. To test this, we calculated the primacy sets for 1000 sparse odor mixtures atop a static background of a low and high intensity, comparing their primacy sets for each mixture. Primacy sets of sufficient size ($p \gtrsim 8$) are almost entirely preserved across odor concentration, indicating that primacy coding, if true, would benefit from universal ORN adaptation in maintaining concentration-invariant odor representations in confounding environments. (Figure forthcoming)

Together, these results suggest that front-end adaptation, in concert with the compressed sensing paradigm, are largely in agreement with the predictions of the primacy coding hypotheses. Our framework also provides the testable prediction that primacy coding may break down for more complex odor mixtures.

E. Cooperative effects of ORN adaptation and downstream normalization. Lateral inhibition among antennal lobe glomeruli normalizes ORN responses prior to their projections to the mushroom body (19, 37). This inhibition obeys a type of divisive gain control, normalizing each input by the sum of ORN activity (20). To what extent does Weber Law adaptation in the olfactory periphery act in tandem with (or counteract) this downstream normalization to maintain odor representations? To investigate this, we extended our

497
498
499
500
501
502
503
504
505
506
507
508
509
510
511
512
513
514
515
516
517
518
519
520
521
522
523
524
525
526
527
528
529
530
531
532
533
534
535
536
537
538
539
540
541
542
543
544
545
546
547
548
549
550
551
552
553
554
555
556
557
558

559
560
561
562
563
564
565
566
567
568
569
570
571
572
573
574
575
576
577
578
579
580
581
582
583
584
585
586
587
588
589
590
591
592
593
594
595
596
597
598
599
600
601
602
603
604
605
606
607
608
609
610
611
612
613
614
615
616
617
618
619
620

Fig. 3. Front-end adaptation promotes accurate sparse odor decoding across concentration changes. **A** Odor stimuli produce ORN responses via odor-binding and activation and firing machinery, as described by Eqs. 1-2. Odors are then decoded using compressed sensing by linearizing around a background s_0 and minimizing the constrained L_1 norm of the odor signal. Odors are assumed sparse, exhibiting K nonzero components, $K \ll N$. **B** Decoding accuracy as a function of odor concentration (a.u.) and odor complexity K, for the non-adaptive and adaptive system respectively. **C** Decoding accuracy of foreground odors in the presence of background odors. Individual plots the decoding accuracy of the foreground as a function of its intensity and complexity, for the given background odor conditions; the intensity of the background odor increases by column and its complexity by row. **D** Same as (C), for the adaptive system.

ORN encoding model by adding uniglomerular connections from ORNs to the antennal lobe, followed by sparse, divergent connections to 2500 Kenyon cells (KCs) in the mushroom body (38–40) (Fig. 5a). Divisive normalization in the AL was modeled via (20):

$$r_{\mathrm{PN},a}(t) = \frac{r_a(t)^{1.5}}{\sigma^{1.5} + r_a(t)^{1.5} + (\gamma \sum_b^M r_b(t))^{1.5}} \quad [4]$$

We then quantified decoding accuracy by training and testing a binary linear classifier on the KC activity output of many sparse odors of distinct intensity and identity, each randomly categorized as appetitive or aversive. Odor signals of the same identity but differing intensity were assigned the same valence (Fig. 5a). We trained the classifier on p sparse odor identities at intensities chosen randomly over 4 orders of magnitude, then tested the classifier accuracy on the same odor identities but of differing concentrations.

Classification accuracy degrades to chance level as the number of distinct odor identities N_{ID} becomes very high (Fig. 5). When acting alone, either divisive normalization or ORN adaptation can mitigate this, although the effect of ORN adaptation is stronger (Fig. 5b). When both are active, accuracy improves further, suggesting that these distinct adaptive transformations may act jointly at different stages of neural processing to preserve representations of odor identity. If odors are instead chosen from a narrower intensity range, performance improves without either adaptive mechanism at play (Fig. 5c). Interestingly, if we train the classifier to distinguish odors by their distinct identity using multiclass categorization (Fig. 5a), we find that the benefits conferred by divisive normalization do not appear until p is substantial, with accuracy below 65%

for $N_{\mathrm{ID}} > 50$ (Fig. 5d). On the other hand, with ORN adaptation accuracy remains above 85% for N_{ID} as high as 1000. Together, this indicates that front-end adaptation plays a key role in maintaining odor identity representations, before they are further normalized and diverged in downstream processing. In some categorization tasks, subsequent normalization can further preserve these representations.

2. Discussion

– also don't forget to mention that the odor-receptor interactions are nonlinear and that saturation is important in this case – also many odors

We investigate, through theory and computations, the implications of recent experimental evidence for a universal mechanism of input gain control in *Drosophila* olfactory receptor neurons. We argue that this mechanism, Weber's Law of psychophysics, plays a key role in preserving neural representations of odor identity at the front-end of the olfactory pathway, prior to further transformations downstream. Input gain control also acts jointly with normalization in the antennal lobe, implicating the importance of signal transformations at multiple steps in the circuit. We support our conclusions using both a decoding scheme that fully reconstructs odor signals from neural response, and a classification scheme that categorizes odors by identity or valence. We find that input gain control is especially central to the discrimination of fluctuating odor signals from potentially saturating odor backgrounds. For single odorants or simple odor mixtures, our results are also consistent with the primacy coding hypothesis, that signals may be fully encoded by the primacy set of earliest activating glomeruli.
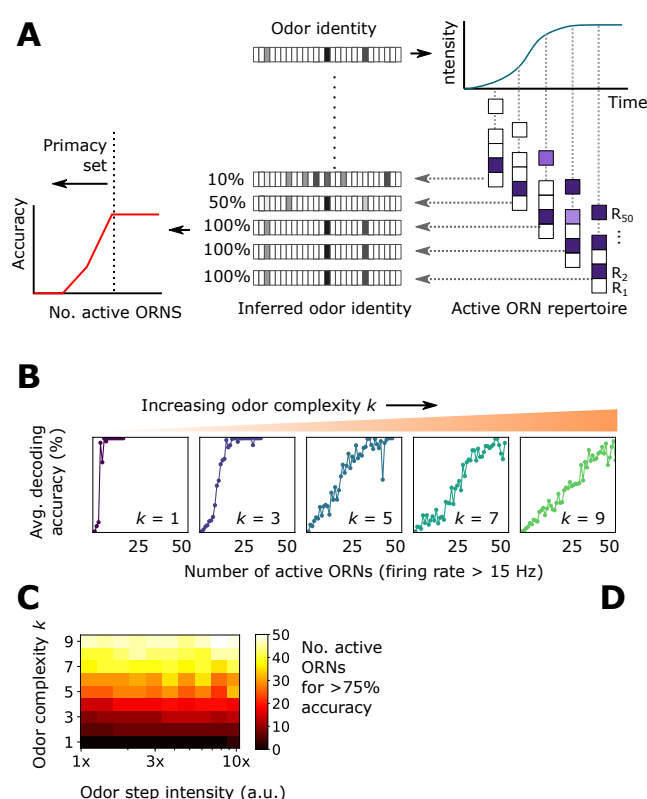
Fig. 4. A Primacy coding posits that only the first p $(p < N)$ active glomeruli are responsible for encoding odor identity. **B** Decoding accuracy as a function of the number of active ORNs (firing rate > 15 Hz), for different odor complexities. **C** Number of active ORNs required to fully decode odor signals of varying odor intensity and complexity. **D** Shift in time to achieve accurate odor identification, as a function of the intensity of odor steps, for various odor complexities (various green-blue lines).

A. Universal front-end adaptation in multi-channel sensory systems. In living systems, sensory adaptation ensures that responses remain in regimes of maximum sensitivity, increasing their effective dynamic range (41–44). Viewing sensory systems as input/output machines, the role of adaptation is therefore to maintain information capacity in dynamic environments (45). Doing so requires matching sensory response to attributes of the environment, either by adapting to specific stimuli or to stimuli statistics (41). In a single-channel system such as bacterial chemotaxis, information capacity is increased by matching the midpoint of the nonlinear dose-response curve, where sensitivity is highest, to mean ligand concentration (45). This is enacted in a robust and dynamic way, through a feedback loop from the activity output of the pathway onto proteins dictating receptor sensitivity (46, 47). It is hypothesized that an analogous feedback loop exists in olfactory receptor neurons, from Orco-mediated Or channel activity onto the free energy of receptor activation (14). This mechanism appears to act identically across ORNs, and because olfactory receptive fields are highly overlapping, raises questions about its efficacy in complex environments: adaptation to one odor could adversely affect identification of a new odor if the latter excites some but not all of the same ORNs. Our results show that this universal mechanism of front-end gain control does help to preserve combinatorial representations of odor identity, despite these broad overlaps.

While Weber-Fechner gain control operates at the level of individual ORNs, lateral inhibition in antennal lobe glomeruli mixes signals among all ORNs (20). We find that olfactory circuits exhibiting both of these adaptive mechanisms outperform systems containing one alone. Combinatorial coding, therefore, benefits both from the separate adaptation of individual single sensory neurons, as well as the normalization of aggregated response. It is notable that both Weber-Fechner adaptation and divisive normalization modulate the location of maximal sensitivity rather than the scale of absolute activity – they move dose-response curves horizontally, rather than stretching them vertically. They are both mechanisms of input gain control rather than response gain control. Such input mechanisms are common to other models, sensory ssytems, etc... (...la).

Other mechanisms in the sensory periphery likely play a role in maintaining neural representations of odor identity. ORNs that contain both excitatory and inhibitory responses to odorants can increase information capacity by exploiting bidirectionality of response (48). Antagonism among odorants, in which multiple odorants compete for common ORN binding sites, could help maintain the sparsity of glomerular activation, provided that binding and activation strengths are uncorrelated (49). This mechanism requires odor-specific activation processes, i.e. G protein-coupled, cAMP-mediated transduction as in mammalian olfaction (Spehr, Munger 2009). We rely instead on experimental evidence for non-ORN-specific and non-odor-specific dynamic gain control acting via the universally expressed co-receptor Orco (Or83b) (14).

B. Odor identification in natural odor environments. Our results are relevant for understanding combinatorial odor coding in naturalistic odor environments. Dynamic gain control acting on a universal timescale of ~ 250 ms allows the of determination of odor identity from single whiffs, particularly when these whiffs are mixed among static backgrounds. The gains afforded by rapid ORN adaptation increase with the strength and complexity of the background odor, suggesting the involvement of ORN adaptation in odor discrimination. Our results indicate that despite the generality in the adaptive mechanism (which also acts on a universal timescale), odor coding capacity and decoding fidelity are greatly enhanced.

Indeed, Add discrimination papers here.

C. Spatiotemporal odor coding and the primacy hypothesis. Previous studies implicate not only the combination of active ORNs but also their distinct temporal patterns as signatures of odor identity (50–53). ORNs modeled on observed features of these temporal patterns form distinct trajectories in low-dimensional projections, projections which cluster by odor identity, much as we have found here (Fig. 2b). Though we do explicitly utilize the temporal history of neural firing in our decoding schemes, the transmission of information over time is implicit in this framework. Because the strength of ORN feedback onto receptor complex activation depends on each ORN's unique tuning curve, odor signals are naturally formatted into temporal patterns that are both odor- and ORN-specific. The response repertoire at a given time is shaped by response history via integral feedback, and the short
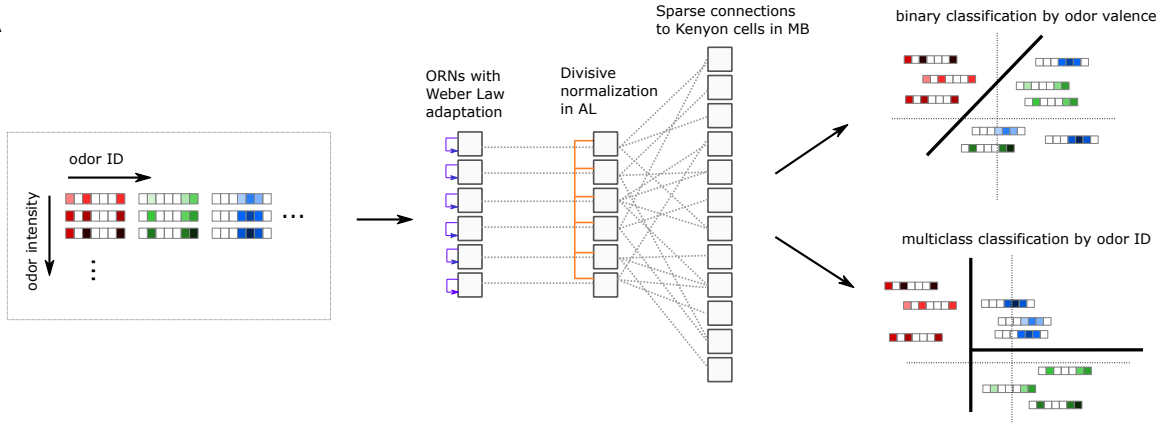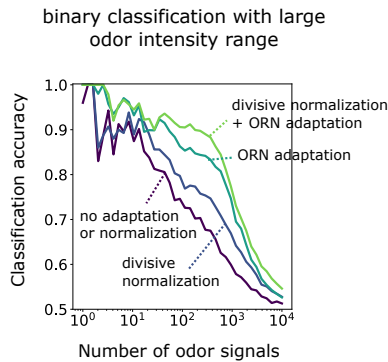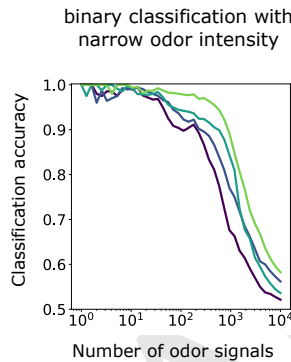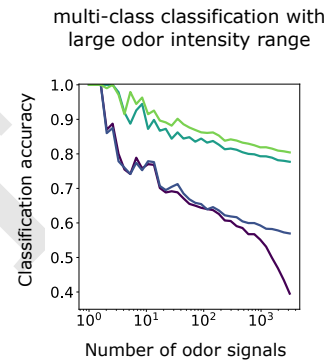
Fig. 5. A Odors of various identity and intensity are encoded by the ORN sensing repertoire (with Weber Law adaptation), which sends signals to glomeruli in the AL, where they are further normalized via lateral inhibition. AL projections neurons then send divergent connections to Kenyon cells in the MB. A linear classifier trains the output of the MB, classifying them either by valence or by odor identity. **B** Accuracy of binary classification by odor valence, as a function of the number of distinct odor identities classified by the trained network (concentrations span 4 orders of magnitude), in systems with only ORN adaptation, only divisive normalization, both or neither. **C** Same as (B), but with concentrations spanning only 1 order. **D**, same as (B) but now classifying in distinct classes by their identity.

forgetting timescales, $\tau_F \sim \tau_A \sim 250$ ms, suggest that only information in brief temporal windows is required for accurate odor identification, consistent with previous findings (52). On the other hand, the classification scheme we employ here (Figs. 5) could ...

Primacy coding also exploits the temporal sequence of glomeruli activation, but in a coarser sense: while the order of ORN activation defines the primacy set, within this set the order is immaterial. We too find that information contained in a primacy subset of the full ORN repertoire can be sufficient for accurate reconstruction of simple odor mixtures. An extension we find, in support of the primacy coding hypothesis, is that primacy sets are also preserved even in the presence of potential confounds such as background odors.

3. Methods

This section needs to be redone

A. Stochastic odor-receptor binding model. We model an odor as an N-dimensional vector $\mathbf{s} = \langle s_1, ..., s_N \rangle$, where $s_i > 0$ are the concentrations of individual volatile molecules (odorants) comprising the odor. In addition, we assume that the odors are sparse in the space of odorants, so only K components of $\mathbf{s}$ are nonzero, where $K \ll N$. The olfactory sensory system is modeled as a collection of M distinct Or/Orco complexes, each of which can be bound with any one of the odorant molecules, and can be either active (firing) inactive (quiescent). We only consider competitive binding, so a complex is bound with one odorant at most. With N possible odorants, receptor a resides in one of $2N + 2$ possible states, $\{R_a, R_a^*, R_a\text{-}s_i, R_a^*\text{-}s_i\}$, indicating receptors that are unbound/inactive, unbound/active, inactive/bound to odorant i, and active/bound to odorant i, respectively. We set $N = 150$ and $M = 50$ throughout.

In the mean-field limit, the binding dynamics of these $2N+2$ states are described by the master equations:

$$\frac{d[R_a\text{-}s_i]}{dt} = k_{ia}^+ s_i [R_a] - k_{ia}^- [R_a\text{-}s_i] \qquad [5]$$

$$\frac{d[R_a^*\text{-}s_i]}{dt} = k_{ia}^{*+} s_i [R_a^*] - k_{ia}^{*-} [R_a^*\text{-}s_i], \qquad [6]$$

when receptor R_a is either inactive (Eq. 5) or active (Eq. 6). Further, transitions between inactive and active states are

described in the mean limit via:

$$\frac{d[R_a]}{dt} = w_a^{\mathrm{u}+}[R_a] - w_a^{\mathrm{u}-}[R_a^*] \tag{7}$$

$$\frac{d[R_a^*\text{-}s_i]}{dt} = w_{ia}^{\mathrm{b}+}[R_a\text{-}s_i] - w_{ia}^{\mathrm{b}-}[R_a^*\text{-}s_i], \tag{8}$$

when receptor R_a is either unbound (Eq. 7) or bound (Eq. 8). The corresponding disassociation constants in terms of the binding transition rates are:

$$K_{ia} = \frac{k_{ia}^-}{k_{ia}^+}$$

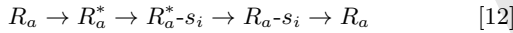$$K_{ia}^* = \frac{k_{ia}^{*-}}{k_{ia}^{+*}} \tag{9}$$

Following (14), we assume that in steady state, the active firing state of an Or/Orco complex is energetically suppressed from the inactive state through corresponding Boltzmann factors:

$$\frac{[R_a^*]}{[R_a]} = \frac{w_a^{\mathrm{u}+}}{w_a^{\mathrm{u}-}} \equiv e^{-\epsilon_a} \tag{10}$$

$$\frac{[R_a^*\text{-}s_i]}{[R_a\text{-}s_i]} = \frac{w_{ia}^{\mathrm{b}+}}{w_{ia}^{\mathrm{b}-}} \equiv e^{-\epsilon_{ia}^{\mathrm{b}}}. \tag{11}$$

These energies are related through detailed balance, which we assume. Applying detailed balance to a given 4-cycle

$$R_a \to R_a^* \to R_a^*\text{-}s_i \to R_a\text{-}s_i \to R_a \tag{12}$$

gives

$$\frac{w_a^{\mathrm{u}+}}{w_a^{\mathrm{u}-}} \frac{k_{ia}^{*+}}{k_{ia}^{*-}} \frac{w_{ia}^{\mathrm{b}-}}{w_{ia}^{\mathrm{b}+}} \frac{k_{ia}^-}{k_{ia}^+} \equiv 1, \tag{13}$$

which, in conjunction with Eqs. 9, 10, and 11, gives

$$\epsilon_{ia}^{\mathrm{b}} = \epsilon_a + \ln\left[\frac{K_{ia}^*}{K_{ia}}\right]. \tag{14}$$

Assuming the binding dynamics are fast, then the probability that receptor a is bound by ligand i when inactive and active can be derived from Eqs. 5 and 6 as

$$p_{ia}^{\mathrm{b}} = \frac{s_i/K_{ia}}{1 + \sum_j^N s_j/K_{ja}} \tag{15}$$

$$p_{ia}^{\mathrm{b},*} = \frac{s_i/K_{ia}^*}{1 + \sum_j^N s_j/K_{ja}^*}. \tag{16}$$

The average activity A_a of complex a is the likelihood that the complex is active, unbound or unbound (equivalantly, the proportion of Or/Orco complexes in a given ORN that are active):

$$A_a = \frac{[R_a^*] + \sum_i^N [R_a^*\text{-}s_i]}{[R_a^*] + \sum_i^N [R_a^*\text{-}s_i] + [R_a] + \sum_i^N [R_a\text{-}s_i]}. \tag{17}$$

Using the master equations between active and inactive states Eq. 7 and 8, this activity obeys the master equation

$$\frac{dA_a}{dt} = w_a^+ (1 - A_a) + w_a^- A_a \tag{18}$$

with effective transition rates

$$w_a^+ = \sum_i^N p_{ia}^{\mathrm{b}} w_{ia}^{\mathrm{u}+} + p_a w_a^{\mathrm{u}} \tag{19}$$

and analogously for w_a^-. Setting Eq. 18 to zero gives the steady state average activity level of ORN a:

$$A_a = \left(1 + e^{\epsilon_a} \frac{1 + \sum_i^N s_i/K_{ia}}{1 + \sum_i^N s_i/K_{ia}^*}\right)^{-1}. \tag{??}$$

B. Generation of binding matrices K_{ia}^*. TODO

C. Compressed sensing decoding of ORN response. We decode ORN responses to infer odor signal identities using an abstraction intended to mimic the neural computations underlying odor identification in the *Drosophila* mushroom body. While we make no assumptions that the compressed sensing (CS) algorithm (or one like it) is being utilized in actuality, this framework nonetheless informs our understanding of how the neural representation of odor identity is maintained or lost when passed through a distributed ORN repertoire. In this sense, CS is somewhat of an upper bound on how well a real neural computation might perform in decompressing ORN responses.

We assume that ORN firing rates are linear in the Or/Orco complex activity; for simplicity we let this transform be the identity. Though subsequent neural circuitry, particularly from the glomeruli in the AL to the Kenyon cells in the MB further mix and scramble these responses, we focus here on the information transfer at the sensory periphery alone. In any case, as demonstrated previously (31), we expect that these neural computations would only improve the representation of neural identity, so we expect no negative ramifications for our findings.

CS addresses the problem of determining a sparse signal from a set of linear measurements, when the number of measurements is less than the signal dimension. Specifically, it is a solution to

$$\mathbf{y} = \mathbf{R}\mathbf{s}, \tag{20}$$

where $\mathbf{s} \in \mathbb{R}^N$ and $\mathbf{a} \in \mathbb{R}^M$ are vectors of signals and responses, respectively, and $\mathbf{R}$ is the measurement matrix. Since measurements are fewer than signal components, then $M < N$, whereby $\mathbf{R}$ is wide rectangular and so Eq. 20 cannot be simply inverted to produce $\mathbf{s}$. The idea of CS is to utilize the knowledge that $\mathbf{s}$ is sparse, i.e.g only K of its components, $K \ll N$ are nonzero. Both the measurements and sparsity are thus combined into a single constrained optimization routine:

$$\hat{s}_i = \arg\min \sum_i^N |s_i| \quad \text{such that} \quad \mathbf{y} = \mathbf{R}\mathbf{s} \tag{21}$$

where $\hat{s}_i$ are the optimal estimates of the signal components and the sum, which is known as the L_1 norm of $\mathbf{s}$, is a natural metric of sparsity.

Importantly, the L_1 norm is a convex operation and the constraints are linear, so the optimization has a unique global minimum. To incorporate the nonlinear response of our encoding model into this linear framework, we assume that the responses are generated through the full nonlinear steady state

response, Eq. **??**, but that the measurement matrix needed for decoding uses a linear approximation of this transformation. Expanding Eq. **??** around $s_0 = s_i - \Delta s_i$ gives

$$A_a \approx A_{a,0} + \Delta A_a \qquad [22]$$

$$\Delta A_a = \sum_i^N R_{ia}\Big|_{s_0} \Delta s_i \qquad [23]$$

$$A_{a,0} = \frac{\sum_1^N s_0/K_{ia}^*}{\sum_1^N s_0/K_{ia}^* + e^{\epsilon_a}} \qquad [24]$$

$$R_{ia}\Big|_{s_0} = \frac{e^{\epsilon_a}/K_{ia}^*}{(\sum_i^N s_0/K_{ia}^* + e^{\epsilon_a})^2}, \qquad [25]$$

where we work in the approximation $K_{ia}^* \ll s_0 \ll K_{ia}$. We assume that the neural system has access to the linearized response, Eq. 25, but must infer the excess signals Δs_i from the excess activity ΔA_a. Corresponding to the CS framework, therefore, $\Delta \mathbf{A} \to \mathbf{y}$, $\Delta \mathbf{s} \to \mathbf{s}$, and $R_{ia}\big|_{s_0} \to \mathbf{R}$. We optimize the cost function in Eq. 21 using sequential least squares programming, implemented in Python through using the scientific package SciPy.

D. Or/Orco energies of activation ϵ_a **and enforcement of Weber's Law.** Free energies are considered receptor-independent throughout, with the exception of dynamically adaptive system in a temporal odor environment (Figs. **??** and **??**). To enforce Weber's Law, we assume the receptor activities feed back onto ϵ_a through the free energies. For the static case, adaptation is perfect, whereby Or/Orco activities are pegged to perfectly adapted values $\bar{A}_a$. Incorporating this into Eq. **??**, and assuming $K_{ia}^* \ll s \ll K_{ia}$, gives

$$\bar{\epsilon}_a = \ln\left(\frac{1 - \bar{A}_a}{\bar{A}_a}\right) + \ln\left(\sum_i^N \frac{s_i}{K_{ia}^*}\right). \qquad [26]$$

Assuming that the excess signals are small, $\Delta s_i < s_0$, this gives

$$\epsilon_a \approx \ln(s_0) + \epsilon_{a,0}, \qquad [27]$$

where $\epsilon_{a,0}$ are receptor-dependent constants. In the static case, we choose these constants such that ϵ_a in both adaptive and non-adaptive systems are equivalent, equal to ϵ_L, at a given low concentration, $s_{0,L}$. Below this concentration, we assume adaptation is not in effect, so $\epsilon_a = \epsilon_L$.

It is important to note that while the linearized gain Eq. 25 utilized by the decoding algorithm appears to rely on ϵ_a, by the above argument ϵ_a can in principle be determined by firing rates alone. That is, ϵ_a is inferred in time through integration of Eq. **??**, which relies only on the current ORN activity.

E. Odor signals. Odor signals $\mathbf{s}$ are N-dimensional vectors presumed sparse whereby only K components, s_k are nonzero, $K \ll N$. The magnitudes of the nonzero components s_k are denoted $s_0 + \Delta s_k$. Here, Δs_k is a random vector, while s_0 is both the center of linearization and, in the case of the adaptive system, the value dictating the strength of adaptive feedback $\epsilon_a \sim \ln\langle s_0 \rangle$.

All the signal intensities are in arbitrary units, as they can be scaled to any range by a corresponding shift in the scales of K_{ia} and K_{ia}^*.

F. Dynamic adaptation. Dynamic adaptation is enforced through

$$\frac{d\epsilon_a(t)}{dt} = \frac{1}{\tau_a}\left[A_a - \bar{A}_a\right]. \qquad [\textbf{??}]$$

The perfectly adapted activity levels $\bar{A}_a$ are determined by evaluating Eq. **??** at a given odor intensity, $s_{0,L}$, corresponding to a minimum stimulus at which adaptation takes effect. The decoding step is assumed instantaneous, so decoded odor identity $\hat{\mathbf{s}}$ is determined by the current value of ϵ_a (which, by virtue of Eq. **??**, is determined by ORN activity a short time prior).

For the simulations with two fluctuating odors (Figs. **??**), the traces shown correspond to the values of s_0 (in blue) and $s_{0,b}$ (orange), where $s_{0,b}$ is the baseline concentration of the background odor components, to which the excess signals $\Delta s_{k,b}$ are added to set the individual odorant concentrations. We choose $\Delta s_{k,b} \sim \mathcal{N}(s_{k,b}/3, s_{k,b}/9)$.

G. Parameter values used in all figures. Parameter values for all of the plots are listed in Table 1.

1. Africa Couto, Mattias Alenius, and Barry J. Dickson. Molecular, anatomical, and functional organization of the drosophila olfactory system. *Current Biology*, 15(17), 2005.
2. Linda Buck and Richard Axel. A novel multigene family may encode odorant receptors: a molecular basis of odor recognition. *Cell*, 65(1):175–187, 1991.
3. Bettina Malnic, Junzo Hirono, Takaaki Sato, and Linda B Buck. Combinatorial receptor codes for odors. *Cell*, 96(5):713–723, 1999.
4. Guirong Wang, Allison F. Carey, John R. Carlson, and Laurence J. Zwiebel. Molecular basis of odor coding in the malaria vector mosquito anopheles gambiae. *Proceedings of the National Academy of Sciences*, 107(9):4418–4423, 2010. ISSN 0027-8424. . URL http://www.pnas.org/content/107/9/4418.
5. John G Hildebrand and Gordon M Shepherd. Mechanisms of olfactory discrimination: converging evidence for common principles across phyla. *Annual review of neuroscience*, 20(1): 595–631, 1997.
6. Elissa Hallem and John Carlson. Coding of odors by a receptor repertoire. *Cell*, 125(1): 143–160, 2006. .
7. Marien de Bruyne, Kara Foster, and John R. Carlson. Odor coding in the drosophila antenna. *Neuron*, 30(2):537 – 552, 2001. ISSN 0896-6273. . URL http://www.sciencedirect.com/science/article/pii/S0896627301002896.
8. Rainer W Friedrich and Sigrun I Korsching. Combinatorial and chemotopic odorant coding in the zebrafish olfactory bulb visualized by optical imaging. *Neuron*, 18(5):737–752, 1997.
9. Rachel I. Wilson. Early olfactory processing in *Drosophila*: mechanisms and principles. *Annual Review of Neuroscience*, 36(1):217–241, 2013.
10. John Murlis. Odor plumes and how insects use them. *Annual Review of Entymology*, 37: 505–532, 1992.
11. MJ Weissburg. The fluid dynamical context of chemosensory behavior. *The Biological Bulletin*, 198(2):188–202, 2000. . PMID: 10786940.
12. Antonio Celani, Emmanuel Villermaux, and Massimo Vergassola. Odor landscapes in turbulent environments. *Phys. Rev. X*, 4:041015, Oct 2014. .
13. Ring T. Cardé and Mark A. Willis. Navigational strategies used by insects to find distant, wind-borne sources of odor. *Journal of Chemical Ecology*, 34(7):854–866, Jul 2008.
14. Srinivas Gorur-Shandilya, Mahmut Demir, Junjiajia Long, Damon A Clark, and Thierry Emonet. Olfactory receptor neurons use gain control and complementary kinetics to encode intermittent odorant stimuli. *eLife*, 6:e27670, jun 2017. ISSN 2050-084X. . URL https://doi.org/10.7554/eLife.27670.
15. M. Renou, V. Party, A. Rouyar, and S. Anton. Olfactory signal coding in an odor background. *Biosystems*, 136:35 – 45, 2015.
16. Guangwei Si, Jessleen K Kanwal, Yu Hu, Christopher J Tabone, Jacob Baron, Matthew E Berck, Gaetan Vignoud, and Aravinthan DT Samuel. Invariances in a combinatorial olfactory receptor code. *bioRxiv*, page 208538, 2017.
17. Shelby A Montague, Dennis Mathew, and John R Carlson. Similar odorants elicit different behavioral and physiological responses, some supersustained. *Journal of Neuroscience*, 31 (21):7891–7899, 2011.
18. Carlotta Martelli, John R. Carlson, and Thierry Emonet. Intensity invariant dynamics and odor-specific latencies in olfactory receptor neuron response. *Journal of Neuroscience*, 33 (15):6285–6297, 2013.
19. K. Asahina, M. Louis, S. Piccinotti, and L. Vosshall. A circuit supporting concentration-invariant odor perception in *Drosophila*. *Journal of Biology*, 8(1):9, 2009.
20. Shawn R. Olsen, Bhandawat Vikas, and Rachel I. Wilson. Divisive normalization in olfactory population codes. *Neuron*, 66:287–299, 2010.
21. M. Papadopoulou, S. Cassenaer, T. Nowotny, and G. Laurent. Normalization for sparse encoding of odors by a wide-field interneuron. *Science*, 332(6030):721–725, 2011.
22. Ernst Heinrich Weber. *EH Weber on the tactile senses*. Psychology Press, 1996.
23. Jon Cafaro. Multiple sites of adaptation lead to contrast encoding in the *Drosophila* olfactory system. *Physiological Reports*, 4(4):e12762, 2016. .

Figure	N	M	K	$\mu_{a,\mathsf{L}}$	$\mu_{a,\mathsf{H}}$	$\nu_{a,\mathsf{L}}$	$\nu_{a,\mathsf{H}}$	$\epsilon_{a,0}$	ϵ_L	ϵ_H	$s_{0,\mathsf{L}}$	s_k	$s_{k,\mathsf{F}}$
1c	200	40	6	$2\cdot10^{-4}$	10^{-3}	10^{-2}	1.0	5.4	5.4	10	-	$\mathcal{N}\left(\frac{s_0}{5},\frac{s_0}{15}\right)$	–
3a	100	50	7	0.5	0.5	0.8	0.8	5.4	3.1	10	10^{-1}	$\mathcal{N}\left(\frac{s_0}{3},\frac{s_0}{15}\right)$	–
3b	100	50	7	0.5	0.6	0.6	0.9	5.4	3.1	10	10^{-1}	$\mathcal{N}\left(\frac{s_0}{3},\frac{s_0}{15}\right)$	—
3c	100	50	7	0.5	0.6	0.6	0.9	5.4	3.1	10	10^{-1}	$\mathcal{N}\left(\frac{s_0}{3},\frac{s_0}{15}\right)$	–
??-??	100	50	7	0.5	0.6	0.6	0.9	5.4	3.1	10	10^{-1}	$\mathcal{N}\left(\frac{s_0}{3},\frac{s_0}{15}\right)$	$\mathcal{N}(1,\frac{1}{5})$
??	100	50	7	0.5	0.6	0.6	0.9	–	–	–	10^{-2}	$\mathcal{N}\left(\frac{s_0}{3},\frac{s_0}{9}\right)$	–
??	100	50	7	0.5	0.6	0.6	0.9	–	–	–	10^{-2}	$\mathcal{N}\left(\frac{s_0}{3},\frac{s_0}{9}\right)$	–

Table 1. Parameters for simulations in all of the figures.

24. Li-Hui Cao, Bi-Yang Jing, Dong Yang, Xiankun Zeng, Ying Shen, Yuhai Tu, and Dong-Gen Luo. Distinct signaling of *Drosophila* chemoreceptors in olfactory sensory neurons. *Proceedings of the National Academy of Sciences*, 113(7):E902–E911, 2016. . URL http://www.pnas.org/content/113/7/E902.

25. Hao Guo and Dean P. Smith. Odorant receptor desensitization in insects. *Journal of Experimental Neuroscience*, 11:1–5, 2017.

26. Hao Guo, Kishore Kunwar, and Dean Smith. Odorant receptor sensitivity modulation in *Drosophila*. *The Journal of Neuroscience*, 37(39):9465–9473, 2017.

27. Christopher D. Wilson, Gabriela O. Serrano, Alexei A. Koulakov, and Dmitry Rinberg. A primacy code for odor identity. *Nature Communications*, 8(1):1477, 2017. .

28. Hamza Giaffar, Dmitry Rinberg, and Alexei A. Koulakov. Primacy model and the evolution of the olfactory receptor repertoire. *biorxiv*, 2018. .

29. L.J.P. van der Maaten and G.E. Hinton. Visualizing high-dimensional data using t-sne. *Journal of Machine Learning Research*, 9:2579–2605, 2008.

30. Leslie B Vosshall, Allan M Wong, and Richard Axel. An olfactory sensory map in the fly brain. *Cell*, 102(2):147 – 159, 2000. ISSN 0092-8674. . URL http://www.sciencedirect.com/science/article/pii/S0092867400000210.

31. Kamesh Krishnamurthy, Ann M. Hermundstad, Thierry Mora, Aleksandra M. Walczak, and Vijay Balasubramanian. Disorder and the neural representation of complex odors: smelling in the real world. *bioRxiv*, doi:10.1101/160382, 2017. .

32. David Donoho. Compressed sensing. *IEEE Transactions on Information Theory*, 52(4):1289–1306, 2006.

33. Emmanuel Candes, Justin Romberg, and Terence Tao. Robust uncertainty principles: Exact signal reconstruction from highly incomplete frequency information. *IEEE Transactions on Information Theory*, 52(2):489–509, 2006.

34. Surya Ganguli and Haim Sompolinsky. Compressed sensing, sparsity, and dimensionality in neuronal information processing and data analysis. *Annual Review of Neuroscience*, 35(1): 485–508, 2012. .

35. C. Pehlevan, A. Genkin, and D. B. Chklovskii. A clustering neural network model of insect olfaction. In *2017 51st Asilomar Conference on Signals, Systems, and Computers*, pages 593–600, 2017.

36. G. Lan, P. Sartori, S. Neumann, V. Sourjik, and Y. Tu. The energy-speed-accuracy tradeoff in sensory adaptation. *Nature physics*, 8(5):422–428, 2012. .

37. Shawn R. Olsen and Rachel I. Wilson. Lateral presynaptic inhibition mediates gain control in an olfactory circuit. *Nature*, 452:952–960, 2008.

38. Alex C. Keene and Scott Waddell. *Drosophila* olfactory memory: single genes to complex neural circuits. *Nature Reviews Neuroscience*, 8:341–354, 2007.

39. Ashok Litwin-Kumar, Kameron Decker Harris, Richard Axel, Haim Sompolinsky, and L.F. Abbott. Optimal degrees of synaptic connectivity. *Neuron*, 93(5):1153 – 1164.e7, 2017. ISSN 0896-6273. . URL http://www.sciencedirect.com/science/article/pii/S0896627317300545.

40. S.J.C. Caron, Vanessa Ruta, L.F. Abbott, and Richard Axel. Random convergence of olfactory inputs in the *Drosophila* mushroom body. *Nature*, 497(4774):113–117, 2013.

41. B. Wark, B. N. Lundstrom, and A. Fairhall. Sensory adaptation. *Current Opinion in Neurobiology*, 17(4):423–429, 2007.

42. Katherine I. Nagel and Allison J. Doupe. Temporal processing and adaptation in the songbird auditory forebrain. *Neuron*, 51(6):845 – 859, 2006. ISSN 0896-6273. . URL http://www.sciencedirect.com/science/article/pii/S0896627306006775.

43. S. B. Laughlin. A simple coding procedure enhances a neuron's information capacity. *Zeitschrift für Naturforschung C*, 36(9-10):910–912, 1981.

44. M. DeWeese and A. Zador. Asymmetric dynamics in optimal variance adaptation. *Neural Computation*, 10:1179–1202, 1998.

45. Ilya Nemenman. Information theory and adaptation. In Michael E. Wall, editor, *Quantitative Biology: From Molecular to Cellular Systems*, chapter 4, pages 73–91. CRC Press, USA, 2012.

46. N. Barkai and S. Leibler. Robustness in simple biochemical networks. *Nature*, 387:913–917, 1997.

47. U. Alon, M.G. Surette, Barkai N., and Stan Leibler. Robustness in bacterial chemotaxis. *Nature*, 397:168–171, 1999.

48. Li-Hui Cao, Dong Yang, Wei Wu, Xiankun Zeng, Bi-Yang Jing, Meng-Tong Li, Shanshan Qin, Chao Tang, Yuhai Tu, and Dong-Gen Luo. Odor-evoked inhibition of olfactory sensory neurons drives olfactory perception in *Drosophila*. *Nature Communications*, 8(1):1357, 2017. .

49. Gautam Reddy, Joseph Zak, Massimo Vergassola, and Venkatesh N Murthy. Antagonism in olfactory receptor neurons and its implications for the perception of odor mixtures. *bioRxiv*, page 204354, 2017.

50. Baranidharan Raman, Joby Joseph, Jeff Tang, and Mark Stopfer. Temporally diverse firing patterns in olfactory receptor neurons underlie spatiotemporal neural codes for odors. *Journal of Neuroscience*, 30(6):1994–2006, 2010. .

51. Nitin Gupta and Mark Stopfer. Insect olfactory coding and memory at multiple timescales. *Current Opinion in Neurobiology*, 21:768–773, 2011. .

52. Stacy L. Brown, J. Joseph, and M. Stopfer. Encoding a temporally structured stimulus with a temporally structured neural representation. *Nature Neuroscience*, 8:1568–1576, 2005.

53. N. Gupta and M. Stopfer. A temporal channel for information in sparse sensory coding. *Neuron*, pages 2247–2256, 2014.